applied sciences

MDPI

Article

Potentiometric Biosensor Based on Artificial Antibodies for an Alzheimer Biomarker Detection

Sónia Claúdia Ribeiro [1], Rúben Fernandes [2,3], Felismina T. C. Moreira [1,4,*] and Maria Goreti Ferreira Sales [1,4,5]

[1] BioMark Sensor Research—ISEP, School of Engineering, Polytechnic Institute of Porto, 4249-015 Porto, Portugal; s.claudia.ribeiro@gmail.com (S.C.R.); goreti.sales@eq.uc.pt (M.G.F.S.)
[2] LaBMI, Laboratory of Medical and Industrial Biotechnology, Polytechnic Institute of Porto, 4249-015 Porto, Portugal; ruben.fernandes@ufp.edu.pt
[3] HEFP, FCS-UFP—Fernando Pessoa Hospital, Faculty of Health Sciences, Fernando Pessoa University, 4249-015 Porto, Portugal
[4] CEB, Centre of Biological Engineering, University of Minho, 4715-000 Braga, Portugal
[5] BioMark, Sensor Research@UC, Department of Chemical Engineering, Faculty of Science and Technology, Coimbra University, 3030-790 Coimbra, Portugal
* Correspondence: ftm@isep.ipp.pt

Abstract: This paper presents a potentiometric biosensor for the detection of amyloid β-42 (Aβ-42) in point-of-care analysis. This approach is based on the molecular imprint polymer (MIP) technique, which uses covalently immobilised Aβ-42 to create specific detection cavities on the surface of single-walled carbon nanotubes (SWCNTs). The biosensor was prepared by binding Aβ-42 to the SWCNT surface and then imprinting it by adding acrylamide (monomer), N,N′-methylene-bis-acrylamide (crosslinker) and ammonium persulphate (initiator). The target peptide was removed from the polymer matrix by the proteolytic action of an enzyme (proteinase K). The presence of imprinting sites was confirmed by comparing a MIP-modified surface with a negative control (NIP) consisting of a similar material where the target molecule had been removed from the process. The ability of the sensing material to rebind Aβ-42 was demonstrated by incorporating the MIP material as an electroactive compound in a PVC/plasticiser mixture applied to a solid conductive support of graphite. All steps of the synthesis of the imprinted materials were followed by Raman spectroscopy and Fourier transform infrared spectroscopy (FTIR). The analytical performance was evaluated by potentiometric transduction, and the MIP material showed cationic slopes of 75 mV-decade^{-1} in buffer pH 8.0 and a detection limit of 0.72 μg/mL. Overall, potentiometric transduction confirmed that the sensor can discriminate Aβ-42 in the presence of other biomolecules in the same solution.

Keywords: amyloid β-42; molecularly imprinted polymers; potentiometric sensor; Alzheimer biomarker

Citation: Ribeiro, S.C.; Fernandes, R.; Moreira, F.T.C.; Sales, M.G.F. Potentiometric Biosensor Based on Artificial Antibodies for an Alzheimer Biomarker Detection. *Appl. Sci.* **2022**, *12*, 3625. https://doi.org/10.3390/app12073625

Academic Editor: Andrei Sarbu

Received: 10 February 2022
Accepted: 29 March 2022
Published: 2 April 2022

1. Introduction

Several peptides/proteins are being considered as potential biomarkers for predicting the early stages of Alzheimer's disease (AD). Numerous clinical studies show that the concentrations of these biomarkers in biological fluids correlate with the progression of early-stage disease [1]. The mechanism driving the progression of AD is related to the formation of senile plaques and neurofibrillary tangles, which are responsible for the death of neurons and lead to memory loss and symptomatic behavioural changes [2–5]. Current hypotheses also include circulating Aβ-42 oligomers as potentially neurotoxic (not just the plaques) [6–12]. The detection of Aβ-42 is based on immunochemical reactions, e.g., conventional ELISAs [13], which are highly sensitive and selective, but time-consuming, unstable, and expensive.

Several biosensors have been described in the literature for the detection of Aβ-42 by electrochemical [14,15], surface plasmon resonance (SPR) [16–21] and field-effect transistor

(FET) [22–25] detection. Electrochemical biosensors have been extensively studied due to their promising properties in terms of scalability and price. This transduction technique has a higher sensitivity and reproducibility compared to other transduction instruments and allows for point-of-care (PoC) analysis [15,26–31], but requires a sensitive and selective antigen recognition material. Antibodies are commonly used as capture and recognition elements [27,32–35]. However, this biological element of recognition has some limitations in terms of its stability, price, and reusability. For this reason, we have developed in this work a plastic antibody for the selective recognition of Aβ-42. Some plastic antibodies for the selective recognition of Aβ-42 have been described in the literature with electrochemical transduction using impedance or square wave voltammetry techniques [14,15,36–39]. To the best of our knowledge, this is the first plastic antibody-based sensor with potentiometric transduction for the detection of AD biomarkers in PoC described in the literature.

Potentiometric sensors have several advantages in terms of simple procedures and highly specific/sensitive properties. Ion-selective electrodes (ISEs) with polymeric-selective membranes and solid-state contact have been used extensively and offer several advantages in terms of their precision, response time, cost of analysis, selectivity and sensitivity over a wide concentration range [40–43]. The development of sensing materials based on molecular imprinting polymer technology (MIP) with the size and charge of a specific ion can lead to precise selective interactions [44,45]. Various immobilization strategies for the integration of MIPs and biosensors have been described in the literature. These include: (i) in situ polymerization (bulk) [46], (ii) epitope method [47] or (iii) surface imprinting with chemical or UV initiation [48,49]. In surface imprinting, the molecules are attached to the surfaces in a layer-by-layer approach. In this strategy, the number of binding sites or cavities tends to increase, which is crucial for reaching the desired detection limit [50,51].

Some nanomaterials, such as carbon allotropes and metallic or magnetic nanoparticles, are used to improve binding sites due to their high surface-to-area ratio [52–54]. Carbon nanotubes (CNTs) are widely used in biosensing as conducting transducers or as carriers for the immobilization of target molecules. CNTs exhibit good properties in terms of their conductivity and high surface-to-area ratio and are an ideal nanomaterial for protein/peptide immobilization [55–61].

Overall, this work describes the synthesis of a plastic antibody for an AD biomarker detection with potentiometric transduction in PoC. The peptide is bound to the surface of SWCNTs that were previously carboxylated. Acrylamide (AAM, functional monomer) and N,N′-methylenebisacrylamide (NNMBA, crosslinker) were then reacted, and polymerization began with the addition of ammonium persulfate (APS, initiator) and TEMED at 38 °C. Finally, the peptide was removed from the polymer matrix by the proteolytic action of proteinase K. In parallel, a similar process was performed without peptide to assemble the NIP material. These sensors were used as electroactive materials in a PVC membrane for potentiometric transduction. Thus, this research presents a new concept for the development of low-cost and sensitive sensor platforms for AD diagnostics in PoC.

2. Materials and Methods

2.1. Apparatus

Potentials were measured using a Crison pH meter GLP 21 (±0.1 mV sensitivity) at room temperature with constant stirring. The output signal was passed to a commutation unit and connected to one of the six outputs, which allowed for synchronized measurements. The setup of the potentiometric cell was as follows: epoxy-graphite | Aβ-42 selective membrane | buffered sample solution of 3-(*N*-morpholino)propanesulfonic acid (MOPS), 1×10^{-3} mol/L, pH 8.0 | AgCl (s) | Ag. An Ag/AgCl electrode served as the reference electrode.

Infrared spectra were recorded using a Nicolet 6700 FTIR spectrometer coupled to an attenuated total reflectance (ATR) and equipped with a Nicolet diamond contact crystal. Raman spectroscopy data were obtained with a Thermo Scientific DXR Raman microscope

equipped with a 532 nm laser. A laser power of 8 mW was left on the sample at a slit aperture of 50 µm.

The SEM analysis was performed using a high-resolution (Schottky) scanning electron microscope with X-ray microanalysis and electron backscattered diffraction analysis: Quanta 400 FEG ESEM/EDAX Genesis X4M.

2.2. Reagents and Solutions

All chemicals were of analytical grade and de-ionized water (conductivity 0.1 µS/cm). 3-Morpholinopropane-1-sulfonic acid (MOPS) from Applichem; Aβ-amyloid 42 (Aβ-42) from GeneScript; SWCNTs, *o*-nitrophenyloctyl (oNPOE), high molecular weight poly (vinyl chloride) (PVC), acrylamide (AAM), N,N′-methylenebisacrylamide (NNMBA), ammonium persulfate (APS), oxalic acid (Oac), N-hydroxysuccinimide (NHS), N-ethyl-N′-(3-dimethylaminopropyl)carbodiimide hydrochloride (EDAC) and sodium chloride (NaCl), creatinine (Crea), albumin (Alb), 2-aminoethyl methacrylate hydrochloride (AEMA), proteinase K and sulfuric acid (H_2SO_4) were purchased from Fluka; tetrahydrofuran (THF) was purchased from Riedel-deHaeen; hydrogen peroxide (H_2O_2) and potassium chloride from MERCK; potassium dihydrogen phosphate (KH_2PO_4) and sodium phosphate dibasic dihydrate (Na_2HPO_4) from Panreac; tetramethylethylenediamine (TEMED) and urea from TLC; and CORMAY serum from Cormay diagnostics.

Phosphate buffer solution (PBS) buffer was prepared with the following composition: NaCl, 8 g/L; KCl, 0.2 g/L, Na_2HPO_4, 1.42 g/L; KH_2PO_4, 0.24 g/L. The pH was adjusted to a value of 8.0. The standard solutions of Aβ-42 were prepared from a successive dilution of the stock solution (0.05 mg/mL) previously prepared in ultrapure water. The MOPS 1.0×10^{-3} mol/L were prepared in deionized water.

The interfering species were prepared in MOPS buffer 1.0×10^{-3} mol/L, pH 8 with the following concentrations: Crea 1.2×10^{-5} g/mL, Alb 5.2×10^{-3} g/mL and urea 4.0×10^{-4} g/mL.

2.3. Synthesis of Biomimetic Materials

2.3.1. SWCNT Oxidation

Briefly, 0.5 g of SWCNT was added to a ten-fold diluted solution of concentrated H_2SO_4:H_2O_2 (4:1). Then, the solution was stirred overnight, centrifuged and washed three times with water. The material was then stirred in PBS buffer, pH 7.2, for 2 h to increase the pH. This procedure was repeated three times. Finally, the nanotubes were oven-dried overnight at 40 °C.

2.3.2. Imprinting Stage

Approximately 10 mg of oxidized SWCNT was suspended in 1.0 mL of deionized water by ultrasonically stirring the mixture for approximately 1 min. Then, 1.0 mL of an aqueous solution containing 5 mmol/L NHS and 2 mmol/L EDAC was added, and the mixture was stirred at room temperature for 45 min. The suspension was then filtered, and the solid was thoroughly rinsed with deionized water to remove unreacted reagents. After activation of the carboxylic acids by EDAC/NHS treatment, 1 mL of 0.01 µg/mL Aβ-42 prepared in MOPs buffer pH 8.0 was added to the modified material for 2.0 h at 4 °C to bind the template. The imprinting phase began with overnight incubation of the modified SWCNTs with 1 mL 5.0×10^{-4} mol/L AEMA. The materials were then washed several times with deionized water. The polymerization phase starts with the addition of 0.5 mL of a monomer (AAM, 5.0×10^{-4} mol/L) and a crosslinker (NNMBA, 1.0×10^{-4} mol/L) to the SWCNTs previously modified with the peptide. After incubation at room temperature for 60 min, 0.5 mL of APS, 1×10^{-4} mol/L and 0.5 mL of TEMED, 10%, solution in MOPS buffer pH 8.0 were added to start polymerization. The polymerization was carried out at room temperature for 2 h. After that, the sensor was washed thoroughly with deionized water. Finally, the template was removed by exposed to proteinase K (500 µg/mL) for 3 h at

37 °C. The imprinted sensor material was washed with phosphate buffer, pH 7.2, to remove the peptide fractions formed by the enzyme treatment, and dried in an oven at 40 °C.

2.4. Preparation of Sensory Membranes

Different compositions of PVC membranes were prepared to evaluate the potentiometric response of the MIP-based sensors. Approximately 0.05 g PVC, 0.06 g plasticizer (oNPOE) and 2.0 mg MIP and NIP were mixed (see Table 1). The mixture was stirred until complete dispersion of the PVC in 3.5 mL THF. These membranes were dropped onto the graphite electrode surface and dried for 48 h. Then, the membranes were conditioned in an Aβ-42, 0.01 µg/mL solution. The electrodes were stored in this solution when not in use.

Table 1. Membrane composition of Aβ-42 sensors casted in 50 mg of PVC and their potentiometric features in 1.0×10^{-2} M MOPS buffer, pH 6 and 8.

pH	Membrane Composition			Weight (mg)	Slope (mV/Decade)	R^2 (n = 3)	LOD (µg/mL)	LLLR (µg/mL)	Response Time (s)
	Active Ingredient	Plasticizer	Additive						
6	MIP/AAM	oNFOE	—	2:60	62.2 ± 1.3	0.970	1.23	1.20	>60
	NIP/AAM	oNFOE	—	2:60	—	0.920	—	—	>60
8	MIP/AAM	oNFOE	—	2:60	75.1 ± 1.0	0.992	0.97	1.20	>60
	NIP/AAM	oNFOE	—	2:60	44.0 ± 1.0	0.970	0.99	0.75	>60

LOD: limit of detection; LLLR: lower limit of linear range.

2.5. Potentiometric Procedures

The analytical performance of the electrodes was evaluated using calibration curves according to IUPAC recommendations. Potentiometric measurements were performed at two pH values (6 and 8), at room temperature, with constant agitation and recording of potentials after stabilization of ±0.2 mV. The e.m.f. value was measured at constant values of ionic strength, and pH. MOPS solution was used for this purpose; aliquots of 0.4 to 15 mL of 1.0×10^{-4} mol/L MOPS were transferred to 0.25 mL of Aβ-42 solution 0.01 µg/mL and 1.75 mL of buffer in a 100 mL beaker. Calibration data for each calibration included limit of detection (LOD), slope, linear ranges and squared correlation coefficient (R^2). Serum samples were analyzed by adding 100-fold diluted commercial human Cormay® serum and an appropriate amount of Aβ-42 standard. The Aβ-42 concentration was calculated from the analytical data of a control calibration curve in serum.

2.6. Selectivity Study

The potentiometric selectivity coefficients were determined by mixed solutions method (MSM). The selectivity of the biosensor was assessed by quantifying LOD of each calibration curve through the presence of an interfering compound [62]. The selectivity coefficients were calculated according to this equation:

$$K^{POT}_{A\beta-42,J} = a_{A\beta42}/(a_J)^{Z_{A\beta42}/Z_J} \quad (1)$$

In Equation (1), a_J is the concentration of interfering species, Z the ionic charges of the interfering ions and $a_{A\beta42}$ the intersection of the extrapolated linear section of the plot Emf vs. the logarithm of Aβ-42 concentration. Alb, Crea and urea were evaluated as interfering species. For this propose, a fixed concentration of interfering species within the physiological level in serum was added as background, while the concentration of primary ion (Aβ-42) was varied. (Crea, 1.2×10^{-5} g/mL), (Alb, 5.2×10^{-3} g/mL) and (urea, 4.0×10^{-4} g/mL) were evaluated as interfering species.

3. Results and Discussion

3.1. Design of the Plastic Antibodies

Herein, a plastic antibody synthesized on the oxidized SWCNT surface was successfully used for Aβ-42 detection with potentiometric transduction. The SWCNTs were selected for this propose due to their large surface area, which promotes an increase in the number of binding sites of the MIP material. The overall process for preparing the MIP involved the attachment of Aβ-42 to the surface of the SWCNTs (Figure 1), filling the vacant places around the Aβ-42 with an appropriate rigid structure and removing the peptide from the polymer. The polymerization steps were carried out under mild conditions in order to guarantee that 3D-structure and electrostatic environment of Aβ-42 remained stable.

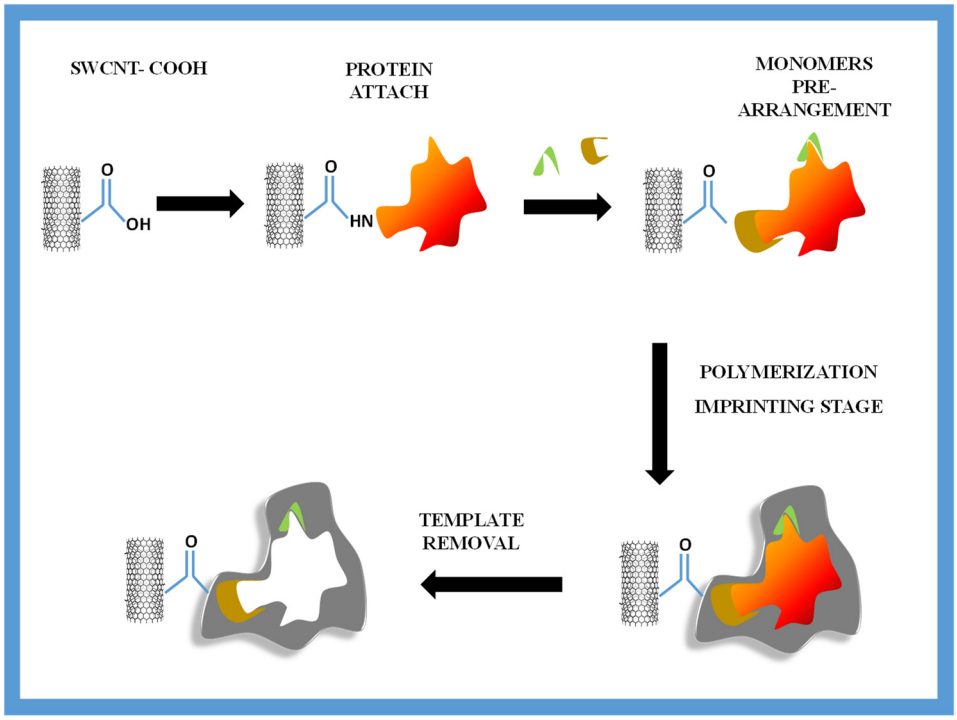

Figure 1. Synthesis of the plastic antibody.

First, the peptide was covalently bound to the previously oxidized SWCNT. The carboxyl groups were activated by an EDAC and NHS reaction. In the first step, a highly reactive *O*-acylurea intermediate is formed [59], which reacts rapidly with NHS to form a more stable ester (succinimidyl intermediate). This ester performs a nucleophilic substitution with any accessible amine group on Aβ-42, leading to the formation of an amide bond between the SWCNTs and Aβ-42.

The formation of stable complexes between the monomers and the target molecule and their preservation in solution are crucial for achieving a suitable selectivity of the imprinting polymer. In this work, electrostatic interactions were established between the target and the monomers. For this purpose, 2-AEMA was used as the functional monomer, forming hydrogen bonds with Aβ-42 [63]. Polymerization then starts with the addition of the monomer AAM, the crosslinker NNMBA and the initiators APS and TEMED after peroxide (OO) bond cleavage by the initiator. Crosslinking between the NNMBA chains was ensured by two terminal vinyl groups. The modified SWCNTs were washed three times with the MOPS buffer [64]. The Aβ-42 was then removed from the polymer by proteinase K treatment. Several washing steps were then performed to remove the free peptide fractions from the surface of the biomimetic material.

3.2. Raman Spectroscopy Studies

The chemical profile of the different materials was evaluated by analysing the Raman spectra. The analysis was performed for the following materials: (i) SWCNT, (ii) SWCNT-COOH and (iii) MIP and NIP. RAMAN spectra give information about the efficiency of the nanotube carboxylation, polymerization and template removal [65].

In general, the structure of the spectrum highlights four distinctive peaks (Figure 2): the first peak in the region around 1300 cm^{-1} (D), the second in the region around 1600 cm^{-1} (G), the third in the high frequencies around 2600 cm^{-1} (G′) and the fourth in the region around 1930 cm^{-1}. Figure 2 shows the Raman spectra for each sample separately, and the ratio of the intensity between G and D band, which is useful for determining the purity of and the degree of the chemical modification of the material. As a result, we observe a significant difference in terms of the peak intensity and shift between different materials. The shifts are essentially perceptible for the G and D bands.

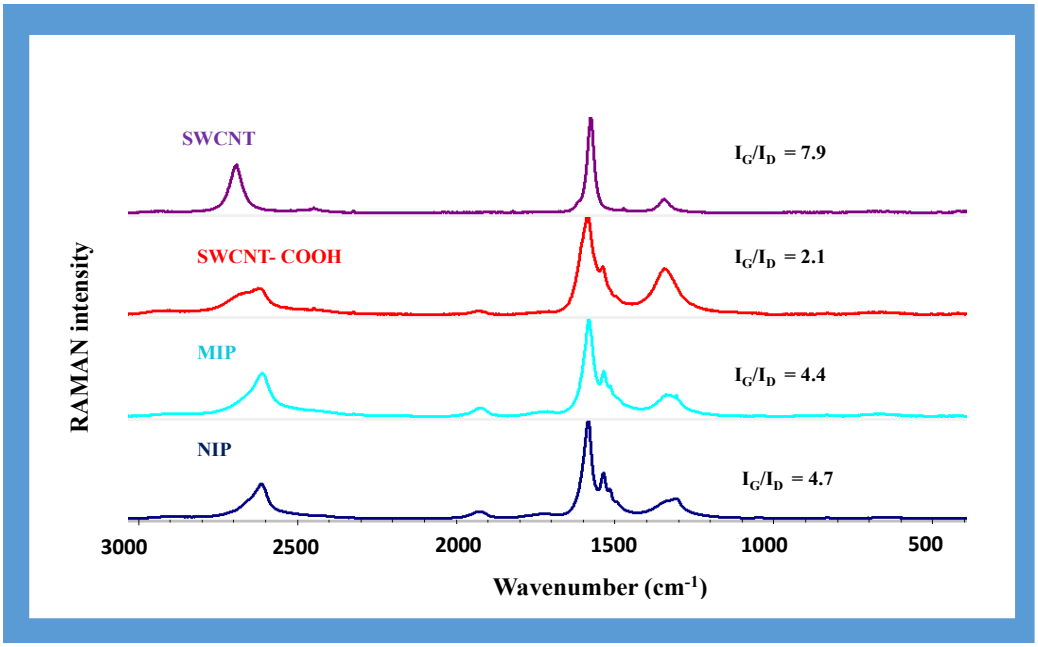

Figure 2. Raman spectra of SWCNT, CNT-COOH and MIP and NIP.

Carbon nanotubes are rolled-up graphene sheets that have been wound into tubes. These nanomaterials are cylindrical tubes with a single outer wall and a diameter typically around 1–2 nm. Due to their exceptional mechanical, electrical and thermal assets, carbon nanotubes are widely used in the field of carbon nanotechnology nowadays.

The Raman spectrum of an SWCNT is similar to graphene, which is to be expected as it is a rolled-up sheet of graphene. In Figure 2, in the Raman spectrum of SWCNT, prominent G and G′ peaks are visible. The band relative to the frequency of tangential displacement (G) is close to 1590 cm^{-1}, and the band associated with the second order peak (G′) is related to the charge transfer between the nanotubes and the reaction mixture [66]. It is also possible to see a well-defined band near 1350 cm^{-1}. This band is denominated as the D band. The D band is ascribed to hybridized vibrational mode, which is related to the graphene edges, and it designates the presence of some disorder to the carbon structure [67].

Comparing the RAMAN spectra of SWCNT and SWCNT-COOH, the latter shows two additional bands near 1540.7 and 267.7 cm^{-1}, and a peak shift of the G′ and G bands approximately 60 and 9 cm^{-1} to the right. These changes are associated with defects in the walls of the nanotubes caused by chemical oxidation by introducing groups (OH, CHO and COOH) on their surface. Additionally, a decrease in the I_G/I_D of the SWCNT after chemical modification from 7.9 to 2.1 was observed, confirming the presence of additional defects in the nanomaterial.

Regarding the RAMAN spectra of MIP and NIP materials, the most relevant information involves changes at the level of the G and D bands and the respective peak ratio (Figure 2). The I_G/I_D for MIP and NIP were 4.4 and 4.7, respectively. These values are very similar, which would be expected, since the polymeric matrix is identical. Besides, this ratio increased in comparison to SWCNT-COOH, indicating the presence of a crystalline structure, since the G band is the Raman signature for sp2 carbons. Additionally, we can observe a shift of the peaks G', G and D to the right compared to the previous step of the chemical modification of SWCNT-COOH, and an enhancement of an additional band at approximately 1900 cm^{-1}. The shift of these bands was approximately 13.9 and 12 cm^{-1}, respectively. Overall, this result confirms the SWCNT oxidation and MIP and NIP polymerization.

3.3. FTIR Analysis

FTIR analysis is useful to evaluate the chemical structure of the nanomaterial and to identify existing compounds by surface analysis. The FTIR / ATR spectra were plotted for SWCNT, SWCNT-COOH, MIP and NIP (Figure 3).

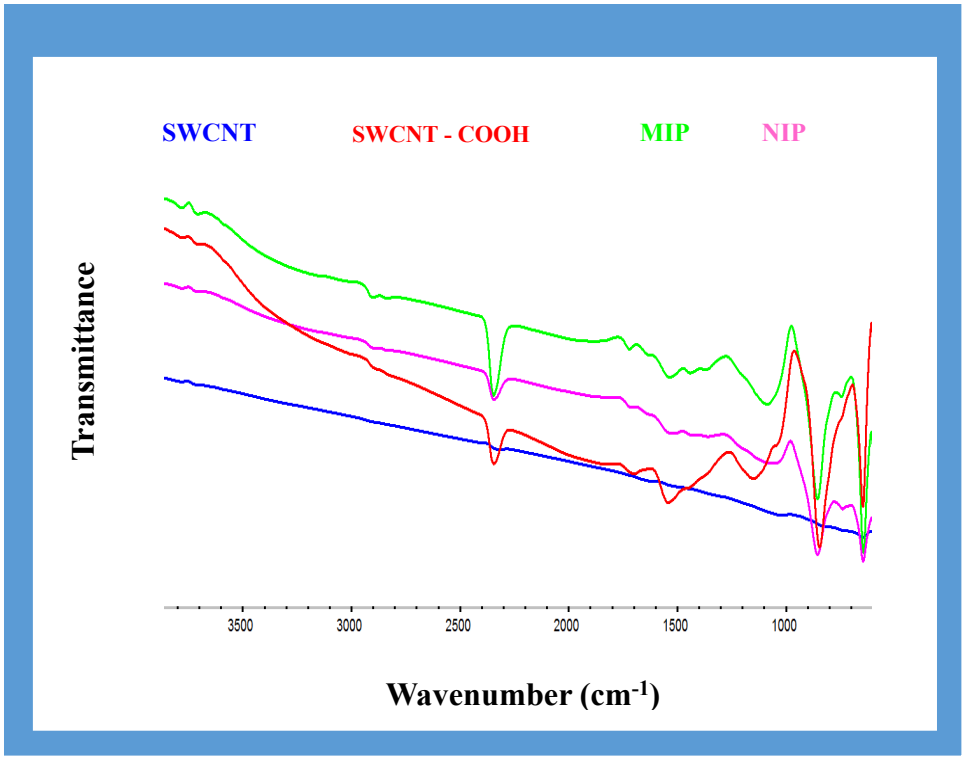

Figure 3. FTIR spectra of SWCNT, CNT-COOH and MIP and NIP.

As observed in Figure 3, the SWCNT does not present relevant visible peaks; however, after acidic treatment, many new peaks appear. The peak observed for SWCNT-COOH at 1701 cm^{-1} can be attributed to the C=O stretch of the carboxylic group, whereas the peak at 1545 cm^{-1} can be related to the C=C stretch of SWCNTs and the peak at 1150 cm^{-1} to the C-O stretch [68,69]. These bands may be related to the chemical oxidation of SWCNT.

Both MIP and NIP materials showed intense peaks at 1723, 1539, 1444, 1087.67 and 856 cm^{-1}, respectively. These peaks have been attributed to the carboxylic/acetone groups, C=C stretch and C-O/C=O stretch bonds. Although these peaks are also present in the SWCNT; however, they showed a peak shift to the left or right. This characteristic allows us to confirm the modification of the surface after polymerization.

3.4. SEM Analysis

The SEM images of the carboxylated SWCNTs and MIP materials are shown in Figure 4. The SWCNTs have a thickness of a few nanometers; however, the SEM images show that the oxidized SWCNTs have some impurities or are in an agglomerated state. The chemical modification of the surface was clearly visible. This was confirmed by magnifying the original material 100,000 times. However, the occurrence of the imprinting could not be verified by SEM, since we cannot observe cavities. In addition, the surface modification with the imprinting polymer significantly increased the thickness of the SWCNT, and some agglomerates were observed, which can be attributed to the presence of the polymer. (see Figure 4).

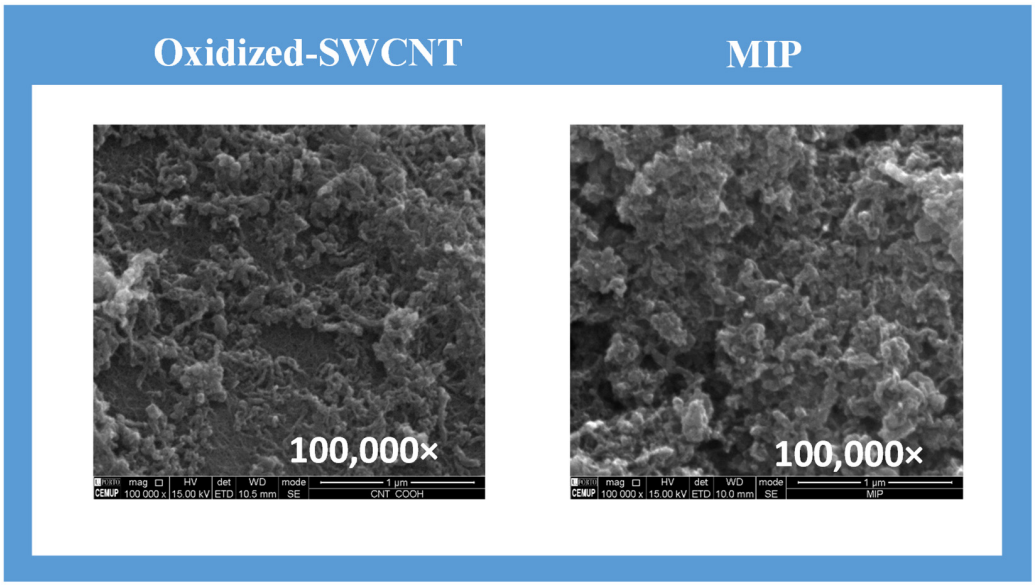

Figure 4. SEM images of oxidized SWCNT and MIP materials.

3.5. Sensory Surfaces

The materials MIP and NIP were incorporated into the PVC membrane and tested as sensing materials with potentiometric transduction. The effect of membrane composition on the potential response was investigated and the results are shown in Table 1.

Overall, the membranes were prepared by dispersing the active compounds (MIP or NIP) in a high dielectric constant plasticizer, oNPOE and PVC. The type of plasticizer employed is important to the analytical performance of PVC-based sensors. Some plasticizers cause leakage or migration from the membrane, which limits the lifetime of sensor materials based on plasticized membranes. Almeida and co-authors have previously described the effects of the plasticizer dielectric constant on the analytical performance of sensors. When oNFOE was used as plasticizing solvent, the detection limit of the sensor was lower due to the higher dielectric constant compared to other conventional solvents [70].

PH Effect

ISEs were calibrated in the MOPS buffer, 1.0×10^{-1} mol/L, pH 6.0 and 8.0. Under these conditions, the peptide is slightly negatively charged because its isoelectric point is 5.5 [64]. However, all electrodes exhibited cationic slopes, and an opposite behavior was expected. A possible explanation for this behaviour is related to the presence of several ionizable functional groups on the amyloid surface that can interact with the PVC membrane, causing the protein to approach the MIP binding sites within the PVC membrane by its positively charged groups. At pH 6, the MIP showed linear behavior after 1.23 µg/mL, a cationic slope of 62.1 mV/dec and a detection limit of 1.20 µg/mL. The NIP showed a nonlinear behavior with an R^2 of 0.92, indicating that the (re)binding mechanism

of the peptide in the imprinted material dominates the potentiometric response (Table 1). Overall, the ISEs with the MIP material showed the best operating characteristics in terms of the slope and R^2.

For the calibration curve at pH 8.0, the MIP sensor showed overnernstian slopes of 75.0 mV/decade and an NIP material of 44.0 mV/decade, respectively. The MIP showed a linear response after 1.20 µg/mL and LOD after 0.97 µg/mL (Figure 5). The particles of NIP showed acceptable properties in terms of LOD, but a lower Nernstian slope compared to the MIP material, indicating that the binding sites of MIP led to the analytical response.

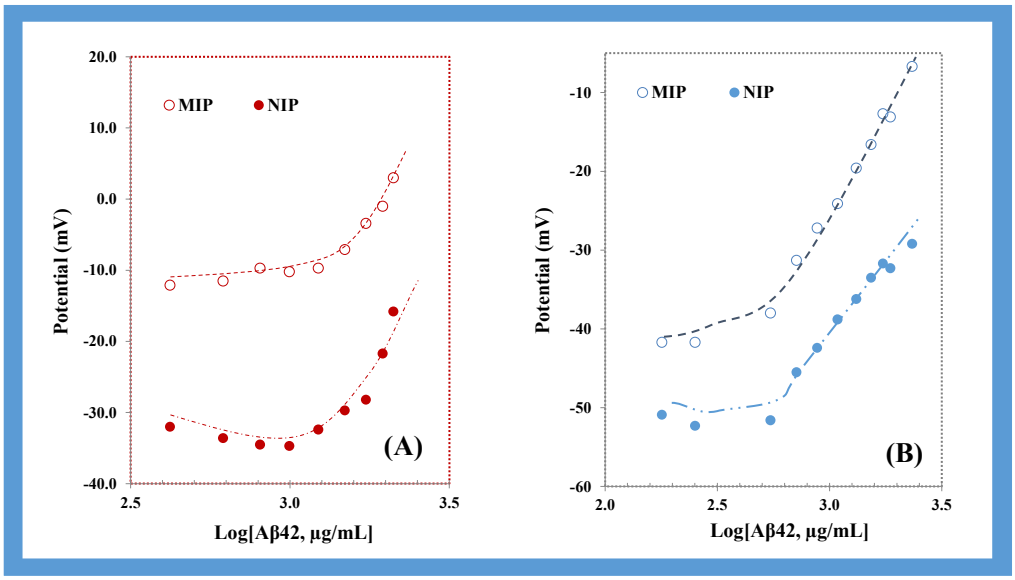

Figure 5. Calibration curve of the ISE-based sensors in MPOS buffer: (**A**) pH 6.0 and (**B**) pH 8.0.

Overall, the best results in terms of the analytical performance were obtained for the membranes with MIP as an ionophore at pH 8.0. These conditions were used for further studies.

The analytical performance of the biosensor was compared (Table S2) with previously reported electrochemical biosensors with different recognition elements for Aβ-42 detection. Overall, these methods show a better analytical performance compared to this approach. However, to our knowledge, this research demonstrates for the first time a simple approach based on potentiometric transduction. We are aware that improvements should be made in terms of the analytical performance. However, we present a low-cost and simple system based on two electrodes made of graphite carbon electrode (reference and working electrode).

3.6. Response Time

The time required to reach a stable potential (±3 mV) in the Aβ-42, 5 µg/mL solution with a rapid 10-fold increase in concentration was 300 s. A low potential drift and long-term stability were observed with successive calibrations. Wash periods with the buffer were inserted between calibrations to remove bound proteins and adjust the potential to a "blank" value. In general, LODs, response times, the linear range and calibration slopes were reproducible within ±5% of their original values over ≈2 weeks.

3.7. Selectivity Study

The selectivity study of ISEs is a critical key factor for the success of the overall performance of the biosensing device in applications in real or close-to-real conditions. There are several methodologies adopted for estimating the potentiometric selectivity coefficients, including the mixed solutions, the separated solutions or the matched potential. Herein, we selected the mixed solution method and tested against the MIP−based ISE

sensor. The selectivity behaviour of Aβ-42 ISEs was estimated by calculating the logarithmic potentiometric selectivity coefficients, log K^{POT}. As the log K^{POT} decreased, the sensor increased its preference for Aβ-42, as these coefficients established the ability of an ISE to differentiate a particular (primary) ion from others (interfering species). The interfering compounds designated for this study were, Crea, Alb and urea prepared in spiked serum. (see Table S1). Overall, a decreased log K^{POT} was expected to be observed for Crea and urea when compared with Alb. As Alb is a protein with many amino acids with functional groups, such as amino and carboxyl groups, and a high molecular weight, an increased log K^{POT} was expected to be observed, and, in contrast, all interfering species were expected to demonstrate quite similar behaviour. This could be ascribed to their net charge at pH 8.0. Thus, the addition of a cationic additive to the membrane is expected to improve the selectivity. However, this study could be conducted in future studies.

3.8. Spiked Serum Samples Analysis

An analytical application of the sensor was performed on the membrane with MIP in a spiked serum sample. Each analysis was performed immediately after the calibration of the ISEs in 100-fold diluted serum.

The concentration of Aβ-42 in serum was 1.31, 1.08 and 0.71 μg/mL, respectively (Table 2). The results obtained for the MIP sensor showed an average recovery of 104.2%, ranging from 102.3% to 107.05%. The relative error ranged from 2.34% to 7.49%. Thus, the results show that the MIP-ISE membranes are suitable for practical use in serum samples. However, the sensor still needs to be improved in terms of the detection limit required to sample analysis.

Table 2. Analytical application of the sensor in spiked serum samples in serum pH 8.0.

[Aβ-42], (μg/mL)	Recovery (%)	Error (%)
1.31	103.5 ± 0.083	3.54 ± 0.08
1.08	107.5 ± 0.22	7.49 ± 0.11
0.71	102.3 ± 0.08	2.34 ± 0.08

4. Conclusions

This research describes the development and characterization of potentiometric sensors based on MIP for the determination of the target molecule Aβ-42.

In essence, MIP technology allows for the production of synthetic receptors with binding constants comparable to those of natural receptors but capable of withstanding extreme conditions, such as temperature, pressure, pH and organic solvents. In theory, synthetic antibodies are very stable and robust, much cheaper than natural receptors and can be stored for long periods of time. The proper selection of the imprinting method is critical, as is the type of polymer material. Conventional bulk imprinting has proven to be a complicated process. Major difficulties include a reduced mass transfer and entrapment of the analyte in the polymer matrix, compromised integrity of the polymer structure, limited solvent choices and formation of heterogeneous binding sites. These limitations can be overcome by surface polymerizations. In surface imprinting, nanometer-sized molecules are immobilized on the surface of nanostructured materials.

In this work, the synthesis of a nanostructured molecular imprint polymer immobilized on a SWCNT surface is described. Due to its small size, a high surface-to-volume ratio is achieved, which favors miniaturization. This material showed good affinity and sensitivity for the Aβ-42 peptide.

The imprinted material was immobilized on a PVC membrane and evaluated by potentiometry. The potentiometric response was controlled by the properties of the medium in which the membranes were located so that the pH had a major influence. In alkaline, more precisely at pH 8.0, the membranes showed good analytical properties. Overall, these membranes have several advantages: a simple design, low response time, and good

selectivity. Moreover, this method proved to be simple, cheap, accurate and cost effective in terms of the reagent and equipment consumption. Further developments are needed to reduce the LOD of the imprinted materials.

Supplementary Materials: The following supporting information can be downloaded at: https://www.mdpi.com/article/10.3390/app12073625/s1, Table S1: Log KPOT for different interfering species in MOPS pH 8.0; Table S2: Electrochemical biosensors for the detection of AD peptide biomarkers using nanomaterials as electrode modifiers or as labels published over the last ten years. References [31,32,39,71–81] are cited in the Supplementary Materials.

Author Contributions: Conceptualization, F.T.C.M. and M.G.F.S.; methodology, S.C.R. validation, S.C.R. formal analysis, F.T.C.M. and S.C.R.; investigation, S.C.R.; resources, F.T.C.M. and M.G.F.S.; writing—original draft preparation, F.T.C.M.; writing—review and editing, F.T.C.M., M.G.F.S. and R.F.; supervision, F.T.C.M., R.F. and M.G.F.S.; project administration, F.T.C.M. and M.G.F.S.; funding acquisition, F.T.C.M. All authors have read and agreed to the published version of the manuscript.

Funding: 0624_2IQBIONEURO_6_E, 2QBioneuro, Impulso de una red de I + i en química biológica para diagnóstico y tratamiento de enfermedades neurológicas EP-INTERREG V A España Portugal (POCTEP).

Institutional Review Board Statement: Not applicable.

Informed Consent Statement: Not applicable.

Data Availability Statement: Not applicable.

Conflicts of Interest: The authors declare no conflict of interest.

References

1. Blennow, K.; Zetterberg, H. Biomarkers for Alzheimer's disease: Current status and prospects for the future. *J. Intern. Med.* **2018**, *284*, 643–663. [CrossRef] [PubMed]
2. Popp, J.; Oikonomidi, A.; Tautvydaitė, D.; Dayon, L.; Bacher, M.; Migliavacca, E.; Henry, H.; Kirkland, R.; Severin, I.; Wojcik, J.; et al. Markers of neuroinflammation associated with Alzheimer's disease pathology in older adults. *Brain Behav. Immun.* **2017**, *62*, 203–211. [CrossRef] [PubMed]
3. Henriksen, K.; O'Bryant, S.E.; Hampel, H.; Trojanowski, J.Q.; Montine, T.J.; Jeromin, A.; Blennow, K.; Lönneborg, A.; Wyss-Coray, T.; Soares, H.; et al. The future of blood-based biomarkers for Alzheimer's disease. *Alzheimer's Dement.* **2014**, *10*, 115–131. [CrossRef] [PubMed]
4. Mapstone, M.; Cheema, A.K.; Fiandaca, M.S.; Zhong, X.; Mhyre, T.R.; MacArthur, L.H.; Hall, W.J.; Fisher, S.G.; Peterson, D.R.; Haley, J.M.; et al. Plasma phospholipids identify antecedent memory impairment in older adults. *Nat. Med.* **2014**, *20*, 415–418. [CrossRef]
5. Doecke, J.D.; Laws, S.M.; Faux, N.G.; Wilson, W.; Burnham, S.C.; Lam, C.-P.; Mondal, A.; Bedo, J.; Bush, A.I.; Brown, B.; et al. Blood-Based Protein Biomarkers for Diagnosis of Alzheimer Disease. *Arch. Neurol.* **2012**, *69*, 1318–1325. [CrossRef]
6. Wang, X.; Wang, L. Screening and Identification of Potential Peripheral Blood Biomarkers for Alzheimer's Disease Based on Bioinformatics Analysis. *Med. Sci. Monit.* **2020**, *26*, e924263. [CrossRef]
7. Chaudhry, A.; Houlden, H.; Rizig, M. Novel fluid biomarkers to differentiate frontotemporal dementia and dementia with Lewy bodies from Alzheimer's disease: A systematic review. *J. Neurol. Sci.* **2020**, *415*, 116886. [CrossRef]
8. Song, Y.; Xu, T.; Zhu, Q.; Zhang, X. Integrated individually electrochemical array for simultaneously detecting multiple Alzheimer's biomarkers. *Biosens. Bioelectron.* **2020**, *162*, 112253. [CrossRef]
9. Kim, K.; Lee, C.H.; Park, C.B. Chemical sensing platforms for detecting trace-level Alzheimer's core biomarkers. *Chem. Soc. Rev.* **2020**, *49*, 5446–5472. [CrossRef]
10. Zetterberg, H.; Burnham, S.C. Blood-based molecular biomarkers for Alzheimer's disease. *Mol. Brain* **2019**, *12*, 26. [CrossRef]
11. Janelidze, S.; Mattsson, N.; Stomrud, E.; Lindberg, O.; Palmqvist, S.; Zetterberg, H.; Blennow, K.; Hansson, O. CSF biomarkers of neuroinflammation and cerebrovascular dysfunction in early Alzheimer disease. *Neurology* **2018**, *91*, e867–e877. [CrossRef] [PubMed]
12. Mayeux, R.; Schupf, N. Blood-based biomarkers for Alzheimer's disease: Plasma Aβ40 and Aβ42, and genetic variants. *Neurobiol. Aging* **2011**, *32*, S10–S19. [CrossRef] [PubMed]
13. Cullen, V.C.; Fredenburg, R.A.; Evans, C.; Conliffe, P.R.; Solomon, M.E. Development and Advanced Validation of an Optimized Method for the Quantitation of Aβ42 in Human Cerebrospinal Fluid. *AAPS J.* **2012**, *14*, 510–518. [CrossRef] [PubMed]
14. Moreira, F.; Rodriguez, B.A.; Dutra, R.A.; Sales, M.G.F. Redox probe-free readings of a β-amyloid-42 plastic antibody sensory material assembled on copper@carbon nanotubes. *Sens. Actuators B Chem.* **2018**, *264*, 1–9. [CrossRef]

15. Moreira, F.T.; Sales, M.G.F. Smart naturally plastic antibody based on poly(α-cyclodextrin) polymer for β-amyloid-42 soluble oligomer detection. *Sens. Actuators B Chem.* **2017**, *240*, 229–238. [CrossRef]
16. Špringer, T.; Hemmerová, E.; Finocchiaro, G.; Krištofiková, Z.; Vyhnálek, M.; Homola, J. Surface plasmon resonance biosensor for the detection of tau-amyloid β complex. *Sens. Actuators B Chem.* **2020**, *316*, 128146. [CrossRef]
17. Nair, R.V.; Yi, P.J.; Padmanabhan, P.; Gulyás, B.Z.; Murukeshan, V.M. Au nano-urchins enabled localized surface plasmon resonance sensing of beta amyloid fibrillation. *Nanoscale Adv.* **2020**, *2*, 2693–2698. [CrossRef]
18. Kim, H.J.; Kim, C.D.; Sohn, Y.S. Thiolated Protein A-functionalized Bimetallic Surface Plasmon Resonance Chip for Enhanced Determination of Amyloid Beta 42. *Appl. Chem. Eng.* **2019**, *30*, 379–383. [CrossRef]
19. Wang, X.Y.; Li, H.; Ma, H.; Seeram, N.; Zhou, F.M. Surface plasmon resonance and related biophysical techniques for the studies of amyloid peptide and protein aggregation and the Inhibition of aggregation by natural products. In *Abstracts of Papers of the American Chemical Society*; American Chemical Society: Washington, DC, USA, 2018; p. 256.
20. Palladino, P.; Aura, A.M.; Spoto, G. Surface plasmon resonance for the label-free detection of Alzheimer's β-amyloid peptide aggregation. *Anal. Bioanal. Chem.* **2015**, *408*, 849–854. [CrossRef]
21. Yi, X.; Feng, C.; Hu, S.; Li, H.; Wang, J. Surface plasmon resonance biosensors for simultaneous monitoring of amyloid-beta oligomers and fibrils and screening of select modulators. *Analyst* **2015**, *141*, 331–336. [CrossRef]
22. Park, H.; Lee, H.; Jeong, S.H.; Lee, E.; Lee, W.; Liu, N.; Yoon, D.S.; Kim, S.; Lee, S.W. MoS2 Field-Effect Transistor-Amyloid-β1–42 Hybrid Device for Signal Amplified Detection of MMP-9. *Anal. Chem.* **2019**, *91*, 8252–8258. [CrossRef] [PubMed]
23. Hideshima, S.; Wustoni, S.; Kuroiwa, S.; Nakanishi, T.; Koike-Takeshita, A.; Osaka, T. Monitoring Amyloid Sup35NM Growth with Label-Free Electrical Detection Using a Field-Effect Transistor Biosensor. *ChemElectroChem* **2013**, *1*, 51–54. [CrossRef]
24. Oh, J.; Yoo, G.; Chang, Y.W.; Kim, H.J.; Jose, J.; Kim, E.; Pyun, J.-C.; Yoo, K.-H. A carbon nanotube metal semiconductor field effect transistor-based biosensor for detection of amyloid-beta in human serum. *Biosens. Bioelectron.* **2013**, *50*, 345–350. [CrossRef] [PubMed]
25. Kim, C.-B.; Chae, C.-J.; Song, K.-B. In Vitro Detection of Beta-Amyloid Peptides using a Photo-Sensitive Field Effect Transistor Integrated with a Single Layer On-Chip Optical Filter. *Biophys. J.* **2012**, *102*, 186a. [CrossRef]
26. Carneiro, M.C.; Moreira, F.T.; Dutra, R.A.; Fernandes, R.; Sales, M.G.F. Homemade 3-carbon electrode system for electrochemical sensing: Application to microRNA detection. *Microchem. J.* **2018**, *138*, 35–44. [CrossRef]
27. Kaushik, A.; Shah, P.; Vabbina, P.K.; Jayant, R.D.; Tiwari, S.; Vashist, A.; Yndart, A.; Nair, M. A label-free electrochemical immunosensor for beta-amyloid detection. *Anal. Methods* **2016**, *8*, 6115–6120. [CrossRef]
28. Liu, L.; Xia, N.; Jiang, M.; Huang, N.; Guo, S.; Li, S.; Zhang, S. Electrochemical detection of amyloid-β oligomer with the signal amplification of alkaline phosphatase plus electrochemical–chemical–chemical redox cycling. *J. Electroanal. Chem.* **2015**, *754*, 40–45. [CrossRef]
29. Negahdary, M.; Heli, H. An ultrasensitive electrochemical aptasensor for early diagnosis of Alzheimer's disease, using a fern leaves-like gold nanostructure. *Talanta* **2019**, *198*, 510–517. [CrossRef]
30. Moreira, F.T.; Sale, M.G.F.; Di Lorenzo, M. Towards timely Alzheimer diagnosis: A self-powered amperometric biosensor for the neurotransmitter acetylcholine. *Biosens. Bioelectron.* **2017**, *87*, 607–614. [CrossRef]
31. Xia, N.; Wang, X.; Zhou, B.; Wu, Y.; Mao, W.; Liu, L. Electrochemical Detection of Amyloid-β Oligomers Based on the Signal Amplification of a Network of Silver Nanoparticles. *ACS Appl. Mater. Interfaces* **2016**, *8*, 19303–19311. [CrossRef]
32. Rama, E.C.; González-García, M.B.; Costa-García, A. Competitive electrochemical immunosensor for amyloid-beta 1-42 detection based on gold nanostructurated Screen-Printed Carbon Electrodes. *Sens. Actuators B Chem.* **2014**, *201*, 567–571. [CrossRef]
33. Miao, J.; Li, X.; Li, Y.; Dong, X.; Zhao, G.; Fang, J.; Wei, Q.; Cao, W. Dual-signal sandwich electrochemical immunosensor for amyloid β-protein detection based on Cu–Al_2O_3-g–C_3N_4–Pd and UiO-66@PANI-MB. *Anal. Chim. Acta* **2019**, *1089*, 48–55. [CrossRef] [PubMed]
34. Lien, T.T.; Takamura, Y.; Tamiya, E.; Vestergaard, M.C. Modified screen printed electrode for development of a highly sensitive label-free impedimetric immunosensor to detect amyloid beta peptides. *Anal. Chim. Acta* **2015**, *892*, 69–76. [CrossRef] [PubMed]
35. Veloso, A.J.; Chow, A.M.; Ganesh, H.V.S.; Li, N.; Dhar, D.; Wu, D.C.H.; Mikhaylichenko, S.; Brown, I.R.; Kerman, K. Electrochemical Immunosensors for Effective Evaluation of Amyloid-Beta Modulators on Oligomeric and Fibrillar Aggregation Processes. *Anal. Chem.* **2014**, *86*, 4901–4909. [CrossRef]
36. Truta, L.A.; Moreira, F.T.; Sales, M.G.F. A dye-sensitized solar cell acting as the electrical reading box of an immunosensor: Application to CEA determination. *Biosens. Bioelectron.* **2018**, *107*, 94–102. [CrossRef]
37. Pereira, M.V.; Marques, A.C.; Oliveira, D.; Martins, R.; Moreira, F.T.C.; Sales, M.G.F.; Fortunato, E. Paper-Based Platform with an In Situ Molecularly Imprinted Polymer for β-Amyloid. *ACS Omega* **2020**, *5*, 12057–12066. [CrossRef]
38. You, M.; Yang, S.; An, Y.; Zhang, F.; He, P. A novel electrochemical biosensor with molecularly imprinted polymers and aptamer-based sandwich assay for determining amyloid-β oligomer. *J. Electroanal. Chem.* **2020**, *862*, 114017. [CrossRef]
39. Özcan, N.; Medetalibeyoglu, H.; Akyıldırım, O.; Atar, N.; Yola, M.L. Electrochemical detection of amyloid-β protein by delaminated titanium carbide MXene/multi-walled carbon nanotubes composite with molecularly imprinted polymer. *Mater. Today Commun.* **2020**, *23*, 101097. [CrossRef]
40. Moreira, F.T.C.; Freitas, V.A.P.; Sales, M.G.F. Biomimetic norfloxacin sensors made of molecularly-imprinted materials for potentiometric transduction. *Mikrochim. Acta* **2010**, *172*, 15–23. [CrossRef]

41. Guerreiro, J.R.; Sales, M.G.F.; Moreira, F.T.C.; Rebelo, T.S.R. Selective recognition in potentiometric transduction of amoxicillin by molecularly imprinted materials. *Eur. Food Res. Technol.* **2010**, *232*, 39–50. [CrossRef]
42. Moreira, F.; Queirós, R.; Truta, L.; Silva, T.I.; Castro, R.M.; Amorim, L.R.; Sales, M.G.F. Host-Tailored Sensors for Leucomalachite Green Potentiometric Measurements. *J. Chem.* **2012**, *2013*, 605403. [CrossRef]
43. Moreira, F.T.; Kamel, A.H.; Guerreiro, R.L.; Azevedo, V.; Sales, M.G.F. New potentiometric sensors based on two competitive recognition sites for determining tetracycline residues using flow-through system. *Procedia Eng.* **2010**, *5*, 1200–1203. [CrossRef]
44. Moreira, F.T.; Kamel, A.H.; Guerreiro, J.R.; Sales, M.G.F. Man-tailored biomimetic sensor of molecularly imprinted materials for the potentiometric measurement of oxytetracycline. *Biosens. Bioelectron.* **2010**, *26*, 566–574. [CrossRef] [PubMed]
45. Blanco-López, M.; Lobo-Castañón, M.; Miranda-Ordieres, A.; Tuñón-Blanco, P. Electrochemical sensors based on molecularly imprinted polymers. *TrAC Trends Anal. Chem.* **2004**, *23*, 36–48. [CrossRef]
46. Henry, O.Y.; Piletsky, S.; Cullen, D. Fabrication of molecularly imprinted polymer microarray on a chip by mid-infrared laser pulse initiated polymerisation. *Biosens. Bioelectron.* **2008**, *23*, 1769–1775. [CrossRef] [PubMed]
47. Steinfeld, U.; Palm, B.D.; Lee, H.H. Polymer Matrix, Process for Their Preparation and Their Use. Patent DE102006040772A1, 20 March 2008.
48. Piletsky, S.A.; Piletska, E.V.; Chen, B.; Karim, K.; Weston, D.; Barrett, G.; Lowe, P.; Turner, A.P.F. Chemical Grafting of Molecularly Imprinted Homopolymers to the Surface of Microplates. Application of Artificial Adrenergic Receptor in Enzyme-Linked Assay for β-Agonists Determination. *Anal. Chem.* **2000**, *72*, 4381–4385. [CrossRef]
49. And, M.-M.T.; Sellergren, B. Thin Molecularly Imprinted Polymer Films via Reversible Addition−Fragmentation Chain Transfer Polymerization. *Chem. Mater.* **2006**, *18*, 1773–1779. [CrossRef]
50. Liang, R.; Ding, J.; Gao, S.; Qin, W. Mussel-Inspired Surface-Imprinted Sensors for Potentiometric Label-Free Detection of Biological Species. Angew. *Chem. Int. Ed.* **2017**, *56*, 6833–6837. [CrossRef]
51. Wang, Y.; Zhou, Y.; Sokolov, J.; Rigas, B.; Levon, K.; Rafailovich, M. A potentiometric protein sensor built with surface molecular imprinting method. *Biosens. Bioelectron.* **2008**, *24*, 162–166. [CrossRef]
52. Golmohammadi, H.; Morales-Narváez, E.; Naghdi, T.; Merkoçi, A. Nanocellulose in Sensing and Biosensing. *Chem. Mater.* **2017**, *29*, 5426–5446. [CrossRef]
53. Su, S.; Wu, W.; Gao, J.; Lu, J.; Fan, C. Nanomaterials-based sensors for applications in environmental monitoring. *J. Mater. Chem.* **2012**, *22*, 18101–18110. [CrossRef]
54. Holzinger, M.; Le Goff, A.; Cosnier, S. Nanomaterials for biosensing applications: A review. *Front. Chem.* **2014**, *2*, 63. [CrossRef] [PubMed]
55. Ji, S.; Lee, M.; Kim, D. Detection of early stage prostate cancer by using a simple carbon nanotube@paper biosensor. *Biosens. Bioelectron.* **2018**, *102*, 345–350. [CrossRef]
56. Khosravi, F.; Loeian, S.M.; Panchapakesan, B. Ultrasensitive Label-Free Sensing of IL-6 Based on PASE Functionalized Carbon Nanotube Micro-Arrays with RNA-Aptamers as Molecular Recognition Elements. *Biosensors* **2017**, *7*, 17. [CrossRef] [PubMed]
57. Li, N.; Wang, Y.; Cao, W.; Zhang, Y.; Yan, T.; Du, B.; Wei, Q. An ultrasensitive electrochemical immunosensor for CEA using MWCNT-NH2 supported PdPt nanocages as labels for signal amplification. *J. Mater. Chem. B* **2015**, *3*, 2006–2011. [CrossRef] [PubMed]
58. Peng, Y.; Wu, Z.; Liu, Z. An electrochemical sensor for paracetamol based on an electropolymerized molecularly imprinted o-phenylenediamine film on a multi-walled carbon nanotube modified glassy carbon electrode. *Anal. Methods* **2014**, *6*, 5673–5681. [CrossRef]
59. Gomes-Filho, S.; Dias, A.; Silva, M.; Silva, B.; Dutra, R.F. A carbon nanotube-based electrochemical immunosensor for cardiac troponin T. *Microchem. J.* **2013**, *109*, 10–15. [CrossRef]
60. Choong, C.-L.; Bendall, J.S.; Milne, W.I. Carbon nanotube array: A new MIP platform. *Biosens. Bioelectron.* **2009**, *25*, 652–656. [CrossRef]
61. Wang, J.; Musameh, M. Carbon-nanotubes doped polypyrrole glucose biosensor. *Anal. Chim. Acta* **2005**, *539*, 209–213. [CrossRef]
62. Bakker, E.; Bühlmann, P.; Pretsch, E. Carrier-Based Ion-Selective Electrodes and Bulk Optodes. General Characteristics. *Chem. Rev.* **1997**, *97*, 3083–3132. [CrossRef]
63. Moreira, F.; Sharma, S.; Dutra, R.A.; Noronha, J.P.; Cass, A.E.; Sales, M.G.F. Smart plastic antibody material (SPAM) tailored on disposable screen printed electrodes for protein recognition: Application to myoglobin detection. *Biosens. Bioelectron.* **2013**, *45*, 237–244. [CrossRef] [PubMed]
64. Moreira, F.; Dutra, R.A.; Noronha, J.P.; Cunha, A.L.; Sales, M.G.F. Artificial antibodies for troponin T by its imprinting on the surface of multiwalled carbon nanotubes: Its use as sensory surfaces. *Biosens. Bioelectron.* **2011**, *28*, 243–250. [CrossRef] [PubMed]
65. Bokobza, L.; Bruneel, J.-L.; Couzi, M. Raman spectroscopy as a tool for the analysis of carbon-based materials (highly oriented pyrolitic graphite, multilayer graphene and multiwall carbon nanotubes) and of some of their elastomeric composites. *Vib. Spectrosc.* **2014**, *74*, 57–63. [CrossRef]
66. Graupner, R. Raman spectroscopy of covalently functionalized single-wall carbon nanotubes. *J. Raman Spectrosc.* **2007**, *38*, 673–683. [CrossRef]
67. Burghard, M. Electronic and vibrational properties of chemically modified single-wall carbon nanotubes. *Surf. Sci. Rep.* **2005**, *58*, 1–109. [CrossRef]

68. Dyke, C.A.; Tour, J.M. Covalent Functionalization of Single-Walled Carbon Nanotubes for Materials Applications. *J. Phys. Chem. A* **2004**, *108*, 11151–11159. [CrossRef]
69. Titus, E.; Ali, N.; Cabral, G.; Grácio, J.; Babu, P.R.; Jackson, M.J. Chemically Functionalized Carbon Nanotubes and Their Characterization Using Thermogravimetric Analysis, Fourier Transform Infrared, and Raman Spectroscopy. *J. Mater. Eng. Perform.* **2006**, *15*, 182–186. [CrossRef]
70. Almeida, S.; Moreira, F.; Heitor, A.; Montenegro, M.; Aguilar, G.; Sales, M. Sulphonamide-imprinted sol–gel materials as ionophores in potentiometric transduction. *Mater. Sci. Eng. C* **2011**, *31*, 1784–1790. [CrossRef]
71. Wu, C.C.; Ku, B.C.; Ko, C.H.; Chiu, C.C.; Wang, G.J.; Yang, Y.H.; Wu, S.J. Electrochemical impedance spectroscopy analysis of A-beta (1-42) peptide using a nanostructured biochip. *Electrochim. Acta* **2014**, *134*, 249–257. [CrossRef]
72. Carneiro, P.; Loureiro, J.; Delerue-Matos, C.; Morais, S.; do Carmo Pereira, M. Alzheimer's disease: Development of a sensitive label-free electrochemical immunosensor for detection of amyloid beta peptide. *Sens. Actuators B-Chem.* **2017**, *239*, 157–165. [CrossRef]
73. Amor-Gutiérrez, O.; Costa-Rama, E.; Arce-Varas, N.; Martínez-Rodríguez, C.; Novelli, A.; Fernández-Sánchez, M.T.; Costa-García, A. Competitive electrochemical immunosensor for the detection of unfolded p53 protein in blood as biomarker for Alzheimer's disease. *Anal. Chim. Acta* **2020**, *1093*, 28–34. [CrossRef] [PubMed]
74. Diba, F.S.; Kim, S.; Lee, H.J. Electrochemical immunoassay for amyloid-beta 1-42 peptide in biological fluids interfacing with a gold nanoparticle modified carbon surface. *Catal. Today* **2017**, *295*, 41–47. [CrossRef]
75. Liu, L.; Zhao, F.; Ma, F.; Zhang, L.; Yang, S.; Xia, N. Electrochemical detection of beta-amyloid peptides on electrode covered with N-terminus-specific antibody based on electrocatalytic O-2 reduction by A beta(1-16)-heme-modified gold nanoparticles. *Biosens. Bioelectron.* **2013**, *49*, 231–235. [CrossRef]
76. Cabral-Miranda, G.; Cardoso, A.R.; Ferreira, L.C.; Sales, M.G.F.; Bachmann, M.F. Biosensor-based selective detection of Zika virus specific antibodies in infected individuals. *Biosens. Bioelectron.* **2018**, *113*, 101–107. [CrossRef] [PubMed]
77. Zhou, Y.; Zhang, H.; Liu, L.; Li, C.; Chang, Z.; Zhu, X.; Ye, B.; Xu, M. Fabrication of an antibody-aptamer sandwich assay for electrochemical evaluation of levels of beta-amyloid oligomers. *Sci. Rep.* **2016**, *6*, 35186. [CrossRef] [PubMed]
78. Qin, J.; Cho, M.; Lee, Y. Ultrasensitive Detection of Amyloid-beta Using Cellular Prion Protein on the Highly Conductive Au Nanoparticles-Poly(3,4-ethylene dioxythiophene)-Poly(thiophene-3-acetic acid) Composite Electrode. *Anal. Chem.* **2019**, *91*, 11259–11265. [CrossRef] [PubMed]
79. Wustoni, S.; Wang, S.; Alvarez, J.R.; Hidalgo, T.C.; Nunes, S.P.; Inal, S. An organic electrochemical transistor integrated with a molecularly selective isoporous membrane for amyloid-beta detection. *Biosens. Bioelectron.* **2019**, *143*, 111561. [CrossRef] [PubMed]
80. Yu, Y.; Sun, X.; Tang, D.; Li, C.; Zhang, L.; Nie, D.; Yin, X.; Shi, G. Gelsolin bound beta-amyloid peptides((1-40/1-42)): Electrochemical evaluation of levels of soluble peptide associated with Alzheimer's disease. *Biosens. Bioelectron.* **2015**, *68*, 115–121. [CrossRef]
81. Qin, J.; Cho, M.; Lee, Y. Ferrocene-Encapsulated Zn Zeolitic Imidazole Framework (ZIF-8) for Optical and Electrochemical Sensing of Amyloid-beta Oligomers and for the Early Diagnosis of Alzheimer's Disease. *ACS Appl. Mater. Interfaces* **2019**, *11*, 11743–11748. [CrossRef]